FULL PAPER

Improvement of polymer properties for powder bed fusion by combining in situ PECVD nanoparticle synthesis and dry coating

Juan S. Gómez Bonilla[1,2,3] 🟢 | Björn Düsenberg[1,2,3] | Franz Lanyi[4] |
Patrik Schmuki[5] 🟢 | Dirk W. Schubert[4,6] | Jochen Schmidt[1,2,3] 🟢 |
Wolfgang Peukert[1,2,3] 🟢 | Andreas Bück[1,2,3] 🟢

[1]Institute of Particle Technology, Friedrich-Alexander-Universität Erlangen-Nürnberg, Erlangen, Germany

[2]Interdisciplinary Center for Functional Particle Systems, Friedrich-Alexander-Universität Erlangen-Nürnberg, Erlangen, Germany

[3]Collaborative Research Center 814 – Additive Manufacturing, Erlangen, Germany

[4]Institute of Polymer Materials (LSP), Friedrich-Alexander-Universität Erlangen-Nürnberg, Erlangen, Germany

[5]Chair of Surface Science and Corrosion, Friedrich- Alexander-Universität Erlangen-Nürnberg, Erlangen, Germany

[6]Bavarian Polymer Institute (BPI), Fürth, Germany

Correspondence
Andreas Bück, Institute of Particle Technology, Friedrich-Alexander-Universität Erlangen-Nürnberg, Cauerstraße 4, D-91058 Erlangen, Germany.
Email: andreas.bueck@fau.de

Abstract

Polypropylene (PP) powders are coated with silica nanoparticles in a fluidized bed to improve the flow behavior of the powders and the processability in powder bed fusion. The nanoparticles are produced in situ via dusty plasma-enhanced chemical vapor deposition (PECVD) in an atmospheric-pressure Ar/O_2 plasma jet fixed at the distributor plate of the fluidized bed. Hexamethyldisiloxane is used as a precursor of the nanoparticles. The influence of the oxygen concentration in the plasma gas and the number of treatment cycles on the chemical composition of the nanoparticles, the amount of nanoparticles deposited, and the flow properties of the coated PP powders is investigated. The chemical composition of the formed silica particles is determined by X-ray photon spectroscopy and infrared spectroscopy. The results reveal that the composition of the nanoparticles is SiO_xC_y, that is, the portion of organic residues introduced by the precursor can be controlled by changing the oxygen concentration in the plasma gas. The mass of nanoparticles deposited on the polymer powder's surface, as determined by inductively coupled optical emission spectroscopy, shows a linear dependence of the number of cycles and the oxygen concentration in the plasma gas. A considerable improvement of the flow behavior of the PP powders is observed after PECVD treatment.
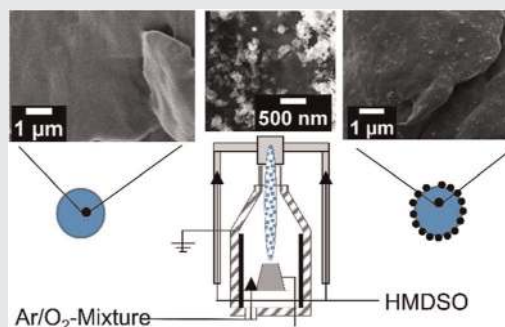
1 | INTRODUCTION

Powder bed fusion (PBF) of polymers is one of several processes that require specific powder properties to produce devices with adequate mechanical properties. This process is an additive manufacturing technique that allows to produce three-dimensional objects layer-wise from a powder bed.[1] In this process, successive powder layers are applied on a building platform where they are heated to a temperature between the melting and crystallization point of the material. A laser scans the powder bed according to a cross-section part geometry defined by a computer-assisted design, providing the energy necessary to melt the particles of the current layer to attach them to the previously melted layer. Polymer powders have to fulfill certain intrinsic and extrinsic powder properties to be suitable for PBF applications, for example, a broad process window (difference between melting and crystallization temperature), sufficient optical absorbance at the wavelength of the laser used, a narrow particle size distribution with a mean particle size between 50 and 80 μm, a near spherical shape, and a good flowability.[2] In particular, the last three mentioned properties are important to assure the spread of continuous and dense layers of powders.

The flowability is defined as the capability of a powder to flow under specific conditions. Powders with a good flowability are especially important, not only for PBF but for many processes of the chemical, food, and pharmaceutical industries, where an accurate dosage and good movement of the powder is required to achieve a high production efficiency and excellent quality of goods.[3,4] The flowability of powders depicts a complex dependence on the powders' bulk properties, surface properties, and process characteristics. It depends, amongst others, on the density of the material, the particle shape and size, moisture content of the material, surface roughness of the powder, as well as on the characteristics of the process, for example, geometry of the equipment and the stress conditions the powder is subjected to in the equipment used.[4-6] The flowability of the powders is directly correlated with the interparticle attractive forces, such as the intermolecular van der Waals forces, local chemical bonds, electrostatic forces, and bridging forces. The magnitude of these forces strongly depends on the surface properties of the powders such as surface texture and roughness, surface

chemistry, and the local contact area upon deformation.[6]

The production of polymer powders with properties required for PBF and with a good flowability is challenging. The forces exerted on the particles during PBF are mainly the weight and the cohesive van der Waals forces. Due to the relative low densities typical of polymers ($> \approx 1 \, \text{g/cm}^3$) and the small particle sizes (50–100 μm), van der Waals forces overcome the weight force of the particles. Hence, fine polymer powders as required for PBF are normally cohesive powders characterized by low packing density and low flowability. Polymer powders have then to be modified to improve the flowability of the powders and to fulfill the requirements of PBF. Methods used to improve the flowability of bulk powders are the particle rounding using mechanical[7] or thermal[8,9] approaches and the increase of the surface roughness of the particles at the nanometer scale by dispersing nanoparticles on the surface,[10-12] with the last one being the most commonly employed. As explained by Rumpf,[13] nanoparticles deposited on the surface act as "spacers," increasing the distance between two surfaces, thus decreasing the magnitude of the van der Waals forces. These nanoparticles are commonly referred to as "flow agents" or "flow conditioners," as they are used to improve the flowability of cohesive materials.[14] Fumed silica nanoparticles are common flow agents used to increase the flowability of polymer powders used in PBF.[12,15] However, the use of nanoparticles can negatively affect the processability of the polymer powders, as they can also act as heterogeneous nuclei for polymer crystals, thus accelerating the crystallization kinetics[16] and narrowing the thermal process window.[17] Hence, only small amounts of flowing agents in the range of 0.1 wt% are typically used.[12,18]

The most commonly used process to achieve the dispersion of nanoparticles on the surface of micron-sized particles is dry particle coating (DPC). During the DPC, the micron-sized particles (referred to as host particles) are brought into collisions with nanoscale particles (referred to as guest particles) by means of mechanical mixing. The guest particles are attached to the surface of the host particles by van der Waals forces.[11,19] Different devices can be used for particle coating,[19,20] where the main difference is in the achieved mixing mechanisms and energy input, and thus the resulting coating kinetics. The optimization of the mixing parameters to obtain an

homogeneous coating with a high degree of coverage depends on the characteristics of used device, and only few empirical correlations have been established.[19] The dry coating also requires additional steps for the production[21] and handling (e.g., drying, storage, transport, packaging) of the (guest) nanoparticles in separated processes before the final application.

Sonnenfeld et al.,[22,23] Spillmann et al.,[14,24] and Roth et al.[25] presented an alternative process to DPC. This process consists of the simultaneous production and deposition of nanoparticles on the surface of the substrate particles by a homogenous gas phase reaction in a dusty plasma-enhanced chemical vapor deposition (PECVD) process. They used a downer reactor provided with a capacitively coupled radio frequency plasma operated at medium vacuum (2 mbar) to deposit SiO_x nanoparticles on cohesive α-D-lactose, high-density polyethylene (PE-HD), and copolyamide powders. In these investigations, hexamethyldisiloxane (HMDSO) was mainly used as a silica organic precursor and Ar/O_2 mixtures were used as the plasma gas. The results obtained showed a considerable increase of the flowability and compressibility of the powders after very short process times (≈0.1 s). The achieved results in terms of powder flowability for lactose (particle size = 6.7 μm) were very close to the ones achieved by conventional DPC.[23] In the case of PE-HD, the dusty plasma treatment led to an increase of the flowability of 57%–80% with respect to the untreated material after process times of about 0.1 s.[23,25] Roth[26] analyzed the effect of the different process parameters (e.g., plasma power, process pressure, gas composition, silicon precursor, mass flow of precursor, powder, etc.) on the plasma properties, the synthesis of nanoparticles, and the modification of the flowability of lactose powders. This plasma process presents several advantages as compared with DPC. The combination of the generation of nanoparticles and coating in one process step avoids the handling of nanoparticles in separated processes. Furthermore, the fast treatment of the powders allows to reduce time and costs.[24,26] According to the recent review on plasma treatment of polymer powders provided by Arpagaus et al.,[27] relatively few studies have been published on the deposition of nanoparticulate spacers using dusty plasma processes, despite the potential of this technique, and these are limited to the abovementioned contributions of the same research group.

In this contribution, the production of silica nanoparticles and coating of polypropylene (PP) micron-sized particles in a fluidized bed reactor provided with an atmospheric-plasma jet are investigated. PP was selected as model material for this investigation, as it is the second most used commodity polymer in the industry and is characterized by its excellent properties such as good fatigue strength and dimensional and chemical stability. PP has also a high potential of applications in PBF due to its broad sintering window in comparison with other commodity polymers as polyethylene that cannot be processed in PBF. The setup employed corresponds to a slightly modified version of the reactor employed for the plasma functionalization of polymer powders reported in previous publications of our group.[28,29] The influence of the plasma gas concentration and duration of the plasma treatment on (1) the chemical composition and amount of SiO_xC_y nanoparticles produced and (2) on the powder bulk properties and flowability of the coated powders is addressed. A comparison with the results obtained using conventional DPC in a tumbling mixer is also provided.

2 | MATERIALS AND METHODS

2.1 | In situ production of nanoparticles and polymer coating

The reactor consists of two main parts: a plasma-enhanced particle generation unit and a fluidized bed, where the coating of the micro-sized particles with the in situ produced nanoparticles takes place.

The particle generation unit is shown in detail in Figure 1. It consists of a crosspiece provided in the lower part with a plasma jet (Openair PFW10; Plasmatreat GmbH). The discharge is generated as a dielectric barrier. The plasma jet is ignited using a frequency of 21 kHz with a power of 4.9 kW. The produced discharge is conducted vertically upward through the crosspiece. The upper end of the crosspiece is connected to a centered orifice in the sintered plate of the fluidized bed, such that the produced nanoparticles are entrained into the fluidized section of the reactor. The two horizontal ends of the crosspiece are used to feed the metal-organic precursor of the desired nanoparticles into the plasma afterglow. For the current investigation, HMDSO (98% purity; Alfa Aesar) was used as an organic precursor for the production of silica nanoparticles. For this purpose, a nitrogen (quality 5.0; Linde AG) flow of 600 ml/min was saturated with the precursor at room temperature using a bubbler. At the tested conditions, this setup led to an evaporation rate of HMDSO of 0.43 g/min (0.56 cm^3/min). The temperature in the fluidized bed is monitored by three centered thermocouples (Type K; TC-Direct) positioned at three different axial positions from the sintered metal plate (10, 130, and 225 mm) directly above the distributor plate.

The reactor characteristics, instruments, and measuring techniques used are outlined in detail
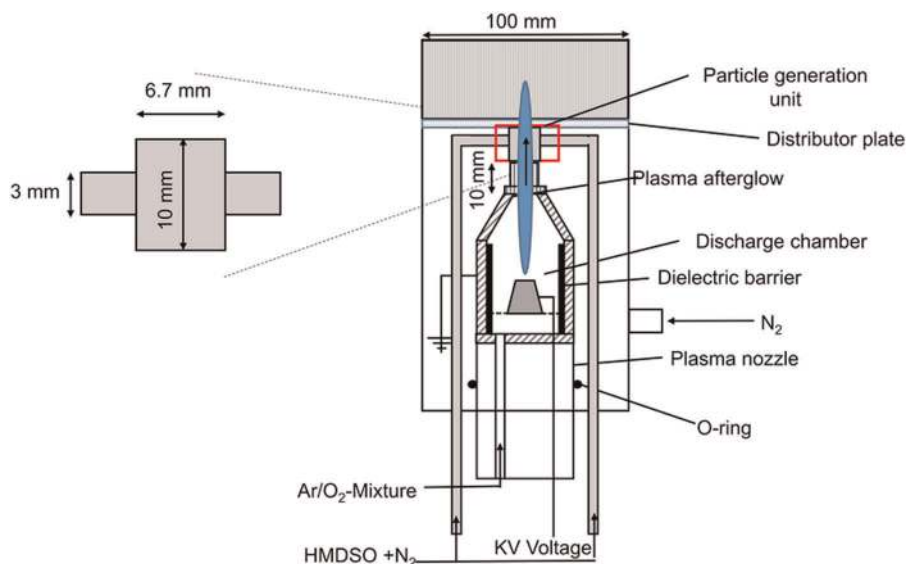
elsewhere.[29] To collect the produced nanoparticles and the fine fraction of the polymer entrained by the fluidization gas from the exhaust, an aramid fiber filter (W. L. Gore & Associates GmbH) was installed in the upper part of the reactor.

In the first step of this investigation, the influence of the oxygen concentration in the plasma gas on the chemical composition of the nanoparticles was investigated. For this purpose, the setup was operated without the addition of polymers to collect nanoparticles for characterization. A sample of the nanoparticles produced was collected in a double-sided carbon tape attached at the first thermocouple of the reactor. To collect a sufficient amount of nanoparticles for the chemical characterization, the plasma was ignited for about 1 h and the produced nanoparticles were collected from the filter. The oxygen concentration in the plasma gas was varied from 0 (pure argon) to 12.5 vol.-%O_2, with increments of 2.5 vol.-%O_2.

For the coating experiments, batches of 300 g PP (Coathylene® PD0580; Axalta Polymer Powders) were treated. The most important properties of the material were determined in previous investigations, and they are listed in Table 1.[29] At the mentioned operating conditions, it was demonstrated that the powder was in a proper fluidized state.

To avoid the melting of the polymer powders at the plasma nozzle, the treatment was conducted in cycles of 60 s plasma, followed by 180 s cooling. This cooling period could be reduced or omitted by installing a cooling system for the plasma nozzle. To investigate the effect of the number of treatment cycles and the oxygen concentration on the quality of the coating and the properties of the powders, these process parameters were varied conse-

quently. The number of cycles was varied between 1 and 15 and the oxygen concentration between 0 and 12.5 vol.-% O_2 according to the values presented in the experiments matrix in Table 2. Higher oxygen concentrations than 12.5 vol.-%O_2 lead to melting of the PP in the fluidized bed, [29] which were thus not investigated.

2.2 | Scanning electron microscopy

The produced nanoparticles as well as the quality of coating were characterized by scanning electron microscopy (SEM). A Gemini Ultra 55 (Carl Zeiss Microscopy GmbH) was used to take images of the particles using SE2 and InLens detectors (acceleration voltage: 1 kV) at ×10,000, ×20,000, and ×40,000 magnification. To decrease the charging effects and to improve the quality of images, the samples were sputter-coated with a thin layer of gold (Hummer JR Technics).

TABLE 1 Material and powder bulk properties of PP Axalta PD0580[29]

Property	Value
Solid density	907 kg/m³
Powder loose packing density	332.1 kg/m³
Sauter diameter	87.8 μm
Flow function ff$_c$ @1300 Pa consolidation	1.39 ± 0.04
Melting temperature (melting peak)	167.37°C
Specific surface area	0.40 m²/g

Abbreviations: ff$_c$, flow function; PP, polypropylene.

TABLE 2 Matrix of experiments

Parameter set reference	Oxygen concentration (vol.- %)	O₂/HMDSO Molar ratio	Number of cycles	PECVD treatment time (min)
1	5	23.5	2	2
2	5	23.5	4	4
3	5	23.5	6	6
4	5	23.5	8	8
5	5	23.5	10	10
6	5	23.5	15	15
7	0	0.0	10	10
8	2.5	11.8	10	10
9	7.5	35.3	10	10
10	10	47.1	10	10
11	12.5	58.9	10	10

Abbreviations: HMDSO, hexamethyldisiloxane; PECVD, plasma-enhanced chemical vapor deposition.

2.3 | Fourier-transform infrared spectroscopy

The nanoparticles collected in the filter were characterized by infrared (IR) spectroscopy to gain information about their chemical structure. IR spectra were recorded in transmission in the spectral range from 4000 to 400 cm^{-1} at a resolution of 2 cm^{-1} using an Fourier-transform infrared (FTIR) spectrometer (Excalibur FTS 3100, Varian Agilent Technologies). To reduce the signal-to-noise ratio, 100 spectral scans were taken for each sample. Sample platelets were prepared by mixing 200 mg dry potassium bromide (UVASol; Merck KGaA) with 1 mg of sample powder. Background and baseline corrections were performed manually. Reported spectra were normalized to their respective maximum absorbance.

2.4 | X-ray photoelectron spectroscopy

The atomic composition of the nanoparticles was analyzed by X-ray photoelectron spectroscopy (XPS; PHI 5600, Physical Electronics, USA). The procedures of sample preparation and measurement employed are described elsewhere.[29]

2.5 | Nitrogen sorption measurements

N₂ adsorption measurements were conducted to determine the mass-specific surface area of the nanoparticles collected in the filter and also determine the Sauter diameter of the primary particle, assuming spherical primary nanoparticles and a density of 2.2 g/cm^3, which is typical of pyrogenic (amorphous) silica nanoparticles. Nitrogen gas sorption analysis was performed using a volumetric gas sorption analyzer Nova4200e (Quantachrome Instruments) The procedure employed for the nitrogen sorption measurements was the same as the reported by Gomez Bonilla.[8]

2.6 | Inductively coupled plasma optical emission spectroscopy

The amount of Si deposited on the samples was determined by inductively coupled plasma optical emission spectroscopy (ICP-OES; Thermo Scientific iCAP 6500), following the procedure described elsewhere.[30] The effective conversion of the precursor was calculated from the thus obtained Si content in the respective samples.

2.7 | Powder flow behavior characterization

A ring shear tester (RST-01.01; Dr. Dietmar Schulze Schüttgutmesstechnik) was employed to measure the flowability of the coated PP powders under different stress conditions, following the same procedure as reported elsewhere.[29] For the measurements, the powders were tested at consolidation stresses of 1425, 2600, and 5232 Pa.

The Hauser ratio defined as the quotient of the powder tapped density and power bulk density was also

determined to characterize the flow behavior of the powders. The tapped density was determined in a measuring cylinder, where 20 g of sample were tapped 1000 times with an automatic tapper (SVM10; Erweka GmbH; Germany) and the finally observed volume was considered.[31]

The loose powder bulk density was determined in the same way as described elsewhere.[29]

2.8 | Dry particle coating

To compare the performance of the described PECVD coating process with other coating techniques, DPC of PP particles with pyrogenic silica (Evonik AG) was carried out in a tumbling mixer (T2f; Willy A. Bachofen AG). Then, 100 g of host particles were mixed with the guest particles at 49 rpm in 1200 ml aluminum bottles, and 190 g of glass beads (Type S; Sigmund Lindner GmbH) with diameters between 0.75 and 1.0 mm were used to promote the deagglomeration of the guest particles and the mixing. The amount of guest particles and the mixing time used in the mixing experiments were adjusted, respectively, to replicate the amount of silica nanoparticles deposited (determined by the ICP-OES measurements) and the PECVD treatment time of the samples produced with the parameter sets 1–6 given in Table 2. Several batches with the same parameters were prepared to obtain a sufficient sample amount for characterization.

2.9 | Differential scanning calorimetry

The effect of the coating process on the crystallization kinetics of PP was assessed by differential scanning calorimetry (DSC) in an isothermal mode. A DSC214 Polyma (NETZSCH-Gerätebau GmbH) was used for the measurements. The isothermal characterization was performed with single measurements. The sample was heated up to 220°C at a rate of 100 K/min and tempered for 1 min to melt the PP completely. The sample was then cooled down to 140°C at a rate of 100 K/min and held for 60 min to observe crystallization at this temperature. By analyzing the isothermal crystallization, conclusions can be drawn about the impact of additives on the crystallization.

3 | RESULTS AND DISCUSSION

3.1 | Synthesis and characterization of SiO_xC_y nanoparticles from HMDSO

Nanoparticles produced at different plasma O_2 gas concentrations collected on a double-sided carbon adhesive tape (at 1 cm above the sintered plate) after 1-min plasma injection are shown in Figure 2. Nanoparticle formation was observed for all the tested plasma O_2 concentrations from 0 to 12.5 vol.-%. The nanoparticles produced can be found as single particles with sizes ranging between 20 and 100 nm as well as large fractal structures composed of several aggregated sintered particles that reached sizes up to 1 μm. The particle size and shape of the deposited particles was found to be similar for all the tested oxygen concentrations. When pure Ar was used as plasma gas, the produced particles were predominantly smaller as compared with the particles produced when oxygen was present in the plasma gas. The number of particles in the aggregates, the size of aggregates, as well as the concentration of particles deposited on the silicon wafer for the same deposition time increase with an increase in the oxygen concentration in the plasma gas. The specific surface area of the nanoparticles produced at different
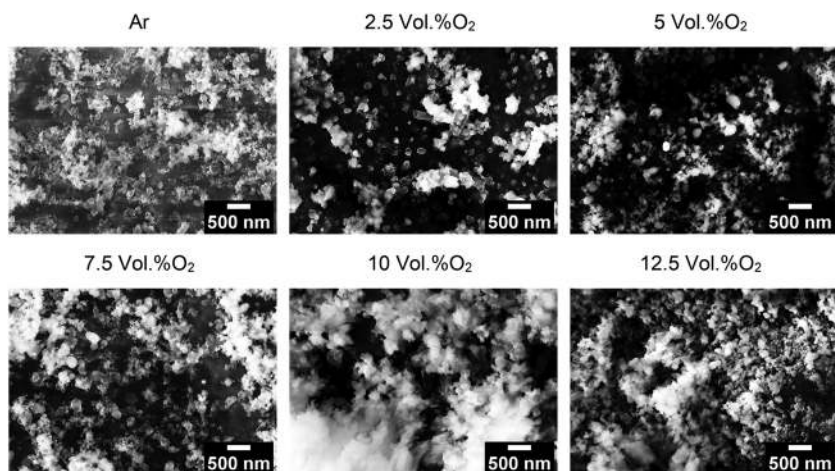

FIGURE 2 Nanoparticles deposited on an Si wafer after 1-min plasma injection for different concentrations of oxygen in the plasma gas
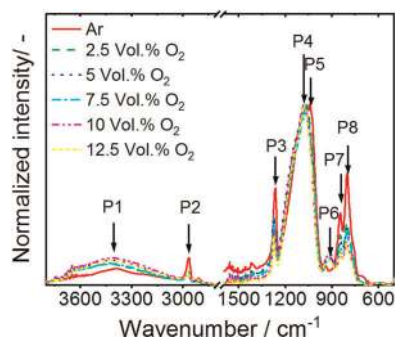
FIGURE 3 Fourier-transform infrared spectra of the produced SiO_xC_y nanoparticles at different oxygen concentrations in the plasma gas

oxygen concentrations is between 23.0 and 25.9 m^2/g, which results in Sauter diameters ranging from 39 to 45.5 nm. The samples show some meso porosity, which can be assigned exclusively to intraparticle porosity, that is, voids within the agglomerates made up of primary particles, such that the determined Sauter diameter is associated with the primary particle size. The size and shape of the single particles were not affected by the concentration of the plasma gas. Similar particles structures were reported by Walliman et al.[32] when using an atmospheric-pressure dielectric barrier discharge reactor for the deposition of SiO_xC_y nanoparticles from HMDSO using Ar–O_2 mixtures as the plasma gas at plasma powers between 0.2 and 11 W.

In the present investigation, the precursor is fed in the afterglow region and not in the discharge region, as in common PECVD processes. Thus, the mechanism of particle formation and growth could be different from those prevailing during classic PECVD. The fragmentation of the precursor molecules and consequent nucleation are more likely to take place as consequence of the moderate gas temperature of the plasma afterglow than as consequence of the collisions with electrons, as in the afterglow, the electron density is considerably lower than in the plasma glow. Similar to the explanation given by Roth et al.,[33] in the initial steps after the fragmentation of the organic precursor, the fragments react with the oxygen radicals present in the plasma afterglow, forming stable chemical compounds resulting in the formation of clusters. The cluster size grows by deposition of precursor reaction products, aggregation, and coagulation, finally resulting in the formation of nanoparticles. After reaching a critical particle size, the nanoparticles stop to grow individually and aggregate with other particles, resulting in the formation of the fractal structures described above.[32,34]

FTIR spectra of the nanoparticles produced at oxygen concentrations in the plasma gas are depicted in Figure 3. The bands considered for the analysis of the chemical structure of the nanoparticles and their corresponding vibrational modes are listed in Table 3.

The dominant absorption band of the nanoparticles is the Si–O–Si (P4, P5) stretching band. This was found at about 1045 cm^{-1} for the nanoparticle produced with pure Ar and it increases progressively with increasing oxygen concentration until reaching 1078 cm^{-1} for 12.5 vol.-%O_2. Similar to the analysis provided by Schäfer et al.,[35] the stoichiometry of the produced SiO_x particles can be derived from the position of the Si–O–Si stretching band by using a linear regression of literature values[36] of the position of the peak and the experimentally determined stoichiometric composition x in SiO_x. The results of this analysis are reported in Table 4. They reveal an increase in the stoichiometry of the SiO_x particles toward the one of SiO_2 from $SiO_{1.65}$ when pure argon was used as plasma

TABLE 3 Assignment of IR absorption bands of the produced nanoparticles

Peak	Wave number (cm^{-1})	Vibrational mode	Reference
P1	3000–3600	O–H stretching	[33,37]
P2	2960	C–H stretching in CH_2 and CH_3	[32,35]
P3	1257	CH_3 s bending in Si–(CH_3)	[35,38]
P4	1075	Si–O–Si stretching network	[35,38]
P5	1010–1035	Si–O–Si stretching suboxide, ring structure	[38,39]
P6	900–960	Si–OH stretching	[39,40]
P7	840	Si–C stretching, CH_3 rocking	[32,38]
P8	808	Si–O–Si bending, Si–C stretching, CH_3 rocking	[32,35,41]

Abbreviation: IR, infrared.

TABLE 4 Chemical composition of silica nanoparticles produced at different oxygen concentrations

Sample	Si–O–Si stretching band (cm^{-1})	x in SiO$_x$	Stoichiometric composition from XPS
Ar	1048	1.65	SiO$_{1.52}$C$_{2.3}$
2.5 vol.-%O$_2$	1067	1.98	SiO$_{1.81}$C$_{1.14}$
5 vol.-%O$_2$	1073	2	SiO$_{1.75}$C$_{1.25}$
7.5 vol.-%O$_2$	1076	2	SiO$_{1.95}$C$_{1.29}$
10 vol.-%O$_2$	1077	2	SiO$_{1.88}$C$_{0.96}$
12.5 vol.-%O$_2$	1078	2	SiO$_{1.95}$C$_{1.03}$

Abbreviation: XPS, X-ray photon spectroscopy.

gas to almost stoichiometric SiO$_2$ with oxygen concentration in plasma gas higher than 5 vol.-%O$_2$.

The C–H stretching band (P2) and CH$_3$ s bending (P3) reveal the presence of CH$_3$ groups for the initial structure of HMDSO. The nanoparticles produced using argon as a plasma gas present the higher intensities of the P2 and P3 bands, indicating a more organic nature with respect to the other samples. With increasing oxygen concentration in the plasma gas, the relative intensity of the aforementioned peaks decreases with respect to the Si–O–Si band. This can be seen more clearly in Figure 4, where the ratio of the Si–CH$_3$/Si–O–Si (P3/P4) is plotted as a function of the oxygen concentration in the plasma gas. The decrease of intensity of the P3 and P1 bands is explained as the decrease of methyl groups in the particles due to oxidation, which results in the production of gaseous compounds like CO$_2$. As a consequence, the carbon content in the particles decreases with an increase in the oxygen concentration in the plasma gas, resulting in more inorganic-like SiO$_x$ nanoparticles.
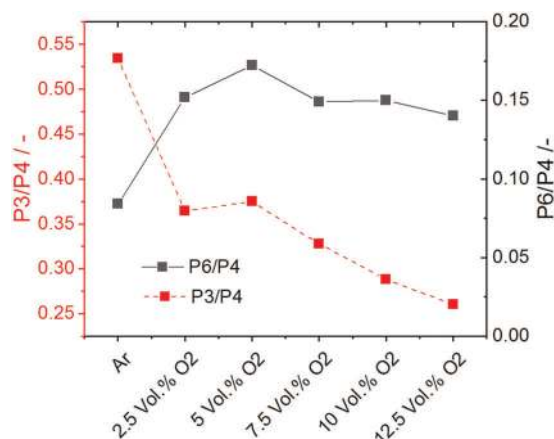
The relative intensity of the Si–OH stretching (P6) and O–H stretching (P1) bands increases significantly when oxygen is present in the plasma gas. This can be observed more clearly in Figure 5, where the ratio of P6/P4 is plotted as a function of the oxygen concentration in the plasma gas. The formation of these peaks implies the formation of silanol groups in the form of associated surface hydroxyl groups, when oxygen is present in the plasma gas.[33,37] The relative intensity of the P6 band seems to be independent of the oxygen concentration.

The chemical composition of the produced nanoparticles is very similar to the results of some of the tested conditions by Wallimann et al.[32] However, the increase of the organic nature (carbon content) of the nanoparticles with oxygen concentration higher than 5% was not observed in the present contribution. In our case, the organic content decreases progressively with the oxygen concentration at least up to an oxygen concentration of 12.5 vol.-%O$_2$. The formation of Si–OH bands was not observed at any of the conditions tested by Walliman.[32]

Table 4 also shows the stoichiometric indices (x and y in SiO$_x$C$_y$) of the produced nanoparticles determined by X-ray photon spectroscopy measurements. The values of x differ from the approximated ones obtained from FTIR,
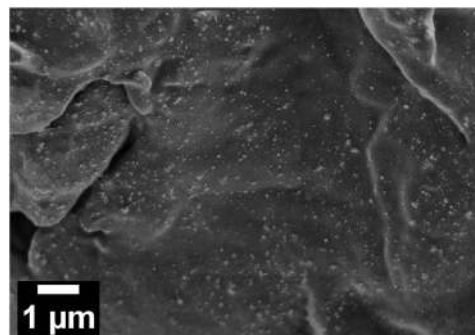

FIGURE 4 Scanning electron microscopy images of polypropylene particles coated with the in-situ produced SiO$_x$C$_y$ particles at 7.5 vol.-%O$_2$ 1 for 10 cycles

FIGURE 5 The band intensity ratio of Si–CH$_3$ (P3) and Si–OH (P6) bands with respect with to Si–O–Si band (P4) as a function of the oxygen concentration in the plasma gas

but the trend observed is similar. When pure argon is used as a plasma gas, the particles present relatively low oxygen stoichiometric x values and considerably high concentration of carbon atoms, corresponding to the relative high amount of CH_3/CH_2 groups identified above. The addition of oxygen in the plasma gas causes a pronounced increase of the oxygen concentration and a decrease of the carbon content relative to Si. Oxygen concentration higher than 7.5 vol.-% leads to x values ranging between 1.88 and 1.95. y Values lower than 1 were obtained for oxygen concentration higher than 10 vol.-%. The atomic concentration of the nanoparticles produced at 10 and 12.5 vol.-%O_2 is very close to the atomic concentration of the nanoparticles reported by Roth et al.[33] using HMDSO as a precursor at 17 vol.-% O_2, an oxygen-to-precursor ratio of 5, and a plasma power of 300 W.

The results presented in this section showed that the presented setup is able to generate nanoparticles with different chemical stoichiometry by changing the composition of the plasma gas, making it possible to produce tailored "organic-like" (hydrophobic) or "inorganic-like" (hydrophilic) nanoparticles. The presented setup, of course, could be applied to produce nanoparticles of other systems (e.g., TiO_2 or Al_2O_3) as well. This is topic of ongoing investigations at our institute.

3.2 | Polymer particle coating

An SEM image showing PP particles coated with the in situ produced nanoparticles (7.5 vol.-%O_2 10 cycles) is given in Figure 4. At the tested conditions, the nanoparticles deposited on the polymer particles present very similar particles size distributions and particle shapes independent of number of plasmas cycles and the oxygen concentration in the plasma gas. At all the tested conditions, a homogenous distribution of the nanoparticles

on the surface of the polymer particles was achieved. It was not possible to obtain particle coating when pure argon was used as plasma gas. This fact is attributed to the low conversion of HMDSO in SiO_xC_y particles in pure Ar plasma.[32]

The nanoparticles deposited on the surface of PP are mostly found as single near-spherical particles of different sizes and also as partial sintered aggregates of few of these single particles. The number-averaged particle size cumulative and density distributions Q_0 and q_0 of the nanoparticles deposited were determined by segmentation and binarization of SEM images, followed by analysis of the particle size using the particle analyzer plugin of ImageJ software.[42] A total of 10,000 nanoparticles were considered for the analysis obtained from SEM images with enough contrast between the polymer surface and the nanoparticles, thus allowing a proper segmentation. Figure 6 shows the obtained particle size distribution as well as an example of the result of the segmentation and binarization procedure applied to the SEM images.

The results presented in Figure 6 show that the size of the nanoparticles deposited on the polymer surface ranges between 14 to 400 nm with number-averaged particle size of $x_{50,0} = 44$ nm. Large fractal structures with particle sizes larger than 500 nm as the deposited ones on the carbon tape were not found on the surface of the polymer particles. The $x_{50,0}$ determined by image analysis (44 nm) is very close to the aforementioned Sauter diameter interval associated with the primary nanoparticles (39.8–45.5 nm) determined by N_2 adsorption measurements. Thus, one can conclude that the surface functionalization process allows to deposit finely dispersed primary particles on the polymer's surface. The size of the structures deposited and the homogeneity of the coating achieved are similar to those obtained when using common DPC of PP[20] and polyethylene[11] particles with commercial Aerosil® at optimal conditions.
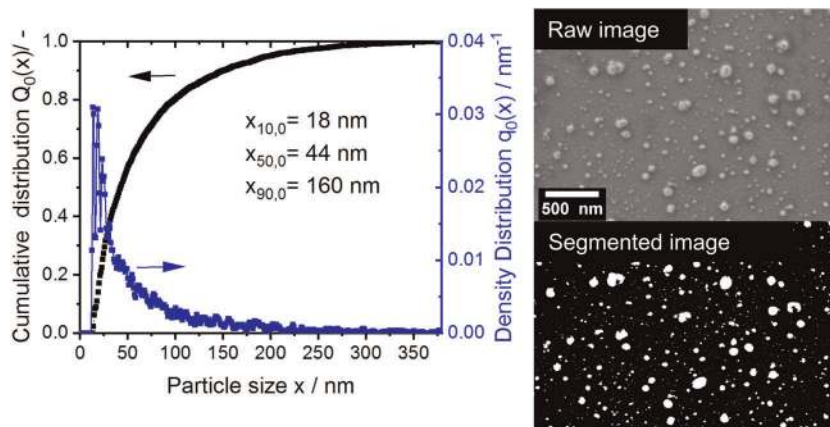

FIGURE 6 Number-averaged particle size distribution of deposited SiO_xC_y particles determined from image processing of scanning electron microscopy images

However, by DPC, the structures were composed of loose agglomerates of several primary particles and not single nanoparticles, as in the presented results.

The nanoparticles attach to the surface of polymer particles due to the predominant adhesive van der Waals forces with respect to the weight and drag forces.[19] The dominance of the van der Waals forces relative to the weight and drag forces acting on the nanoparticles would decrease with increasing size of the nanoparticles, such that at a critical size, the nanoparticles would not attach on the surface and would be entrained by the fluidization gas in the fluidized bed. Redispersion of nanoparticles as consequence of collisions between the polymer particles certainly takes place during fluidization. In this case, bigger nanoparticles are more prone to detach from the surface than the small ones due to lower relative van der Waals forces. Furthermore, as explained by Anh Ho et al.,[43] the higher agglomeration rate between small particles (nanoparticles) and bigger particles (polymer particles), which act as collectors, makes it more probable that the small nanoparticles "agglomerate" on the surface of the polymer particles as compared with the lower agglomeration rate between the big particles (aggregates of nanoparticles and the polymer particles).

The powders collected in the filter after a coating experiment are composed of the fine fraction of the polymer powder and nondeposited SiO_xC_y particles, which were entrained by the fluidization gas. A sample of the powders was dispersed in distilled water and allowed to rest for 2 days, such that the polymer particles and the SiO_xC_y particles separated by sedimentation. Measurements by dynamic light scattering of the supernatant reveal the presence of big agglomerates, which hinder the analysis by means of this method. A sample of the sediment was taken with a plastic pipette and was spread on a silicon wafer. After drying, the sample was analyzed with SEM. The results of this analysis are presented in Figure 7 for a sample taken from the filter after an experiment carried out at 2.5 vol.-%O_2. Under these conditions, the SiO_xC_y particles are predominantly found as big fractal structures and in a minor amount as single small particles. This result supports the findings presented above in which the polymer particles are only coated with the smallest produced nanoparticles, whereas the aggregates or their agglomerates (as well as some of the single particles) are mainly entrained by the fluidization gas.

The amount of silicon deposited on the PP powders for different process conditions was determined by ICP-OES measurements. The amount of nanoparticles deposited on the polymers was expressed as equivalent mass amount of stoichiometric SiO_2. The effective conversion was calculated according to Equation (1):
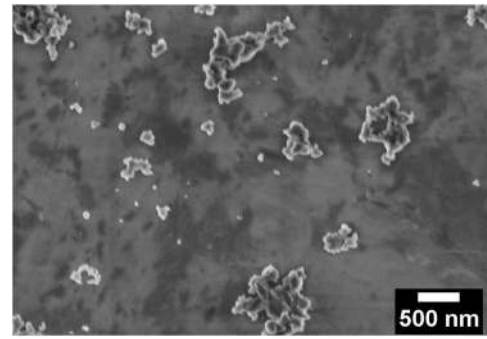

FIGURE 7 SiO_xC_y particles collected in a filter after coating experiments

$$\text{Effective conversion} = \frac{c \frac{mgSi}{gpolymer} \times \frac{m_{\text{polymer}}}{N}}{\dot{m}_{\text{HMDSO}} \times \frac{2 \times M_{si}}{M_{\text{HMDSO}}} \times t_{\text{pcycle}}},$$

(1)

where c is the amount of silicon deposited on the polymer determined from the ICP-OES measurements, m_{polymer} is the batch size (300 g in this investigation), N is the number of plasma cycles, $\dot{m}_{\text{HMDSO}}$ is the mass flow of evaporated HMDSO in the bubbler, M_{si} and M_{HMDSO} are the molecular weights of silicon and HMDSO, respectively, and t_{pcycle} is the duration of a plasma cycles (1 min in this investigation). The effective conversion takes into account the amount of silicon fed as HMDSO, which was effectively converted to SiO_xC_y particles and deposited on the surface of the polymer particles. The effective conversion does not represent the total conversion of HMDSO in silica-like particles, as a large number of the nanoparticles produced were entrained by the fluidization gas out of the fluidized bed, as explained above, or deposited on the walls of the reactor.

The amount of silica nanoparticles deposited on the polymer particles and the effective conversion of the
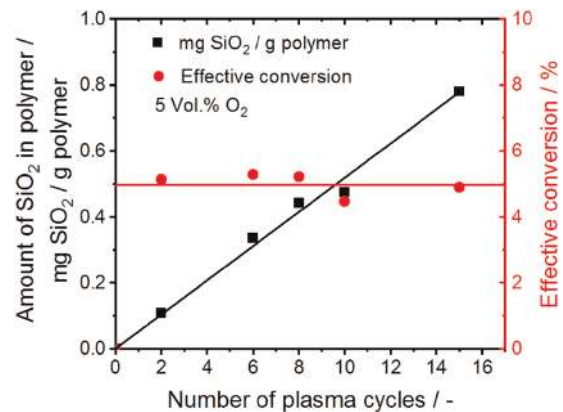

FIGURE 8   Amount of nanoparticles deposited on polypropylene particles and effective conversion as a function of the number of plasma cycles
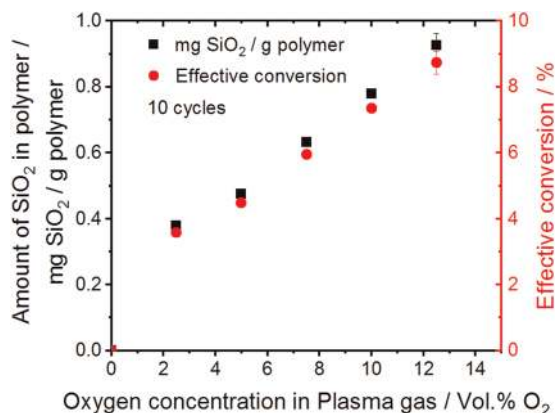
FIGURE 9 Amount of nanoparticles deposited on polypropylene particles and effective conversion as a function of the oxygen concentration in the plasma gas

FIGURE 10 Arrhenius plot of the amount of Si deposited on the polymer particles and the gas temperature measured at the first thermocouple during plasma injection for different oxygen concentrations

process as a function of the number of plasma cycles when using a constant concentration of oxygen of 5% are shown in Figure 8. The amount of deposited nanoparticles increases linearly with increasing number of plasma cycles with a rate of 0.0518-mg nanoparticles/g polymer per cycle. The effective conversion of the process was determined to be independent of the number of cycles with a value of about $5 \pm 0.29\%$. A linear increase in the amount of nanoparticles deposited on PP with increasing number of plasma cycles and a constant effective conversion are also expected when using other oxygen concentrations in the plasma gas.

Figure 9 shows the amount of nanoparticles deposited on the PP particles and the effective conversion of the process for different oxygen concentration after 10 plasma cycles. Both the amount of nanoparticles and the effective conversion increase linearly with an increase in the oxygen concentration in the plasma gas. The amount of nanoparticles deposited with pure Ar as a plasma gas was 0. An effective conversion of about 9% was reached when using an oxygen concentration of 12.5 vol.-%.

The increase of the effective conversion of the process is correlated to the increase of conversion of HMDSO with the oxygen concentration in the plasma gas. The latter can be explained by two main reasons. On the one hand, when the oxygen concentration in the plasma gas increases, the oxygen-to-precursor ratio is also increased. As HMDSO requires oxygen to produce SiO_x particles, higher O_2-to-HMDSO ratios result in an increase in the conversion of HMDSO.[33] On the other hand, a higher concentration of oxygen in the plasma gas leads to higher gas temperatures in the plasma afterglow. The increase of the gas temperatures could enhance the thermal decomposition of the precursor and thus increase the conversion of the process. To represent the dependence of the effective conversion of the process on the gas
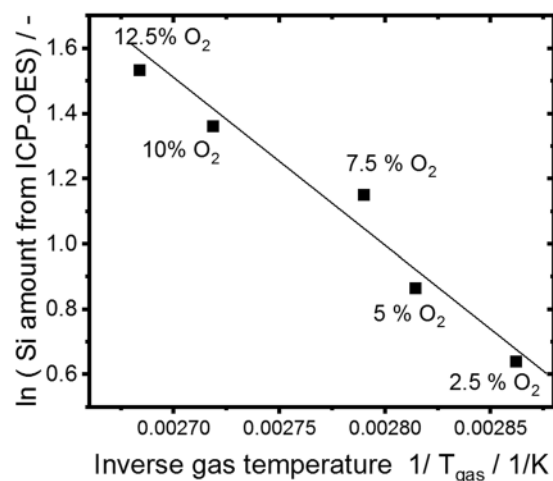
temperature, the natural logarithmic of the Si moles deposited on 300 g of polymer (ln(Si)) determined by ICP-OES was plotted against the reciprocal of the gas temperature $(1/T(K))$ measured during the plasma ignition upon the injection of HMDSO at the first thermocouple (when the fluidized bed was empty and with no fluidization gas). The results are shown in Figure 10. The dependence between the aforementioned quantities can be described by a straight line in the Arrhenius-like plot. This result clearly shows that effective conversion of the process is influenced by the gas temperatures as a consequence of the increasing oxygen amount in the plasma gas.

The presented results differ from the result reported by Wallimann et al.,[32] who found an initial increase of the conversion of HMDSO into SiO_xC_y particles from 0% to 55% when increasing the oxygen concentration from 0 to 2 vol.-%O_2. A further increase of the oxygen concentration leads to a decrease in the conversion, reaching approximately 8% at 10 vol.-%O_2. The decrease of the conversion of HMDSO at elevated oxygen concentration was explained by the formation of ozone and the consequence reduction of dissociation potential in the plasma. The difference between the two investigations can be due to differences in the setup and the prevailing mechanism of particle generation and growth, that is, particle generation and growth in the discharge zone[32] versus particle generation and growth in the afterglow zone (this study).

Considering the linear dependencies of the amount of deposited SiO_xC_y nanoparticles on the number of plasma cycles and the oxygen concentration in the plasma gas shown in Figures 9 and 10, it is possible to derive a
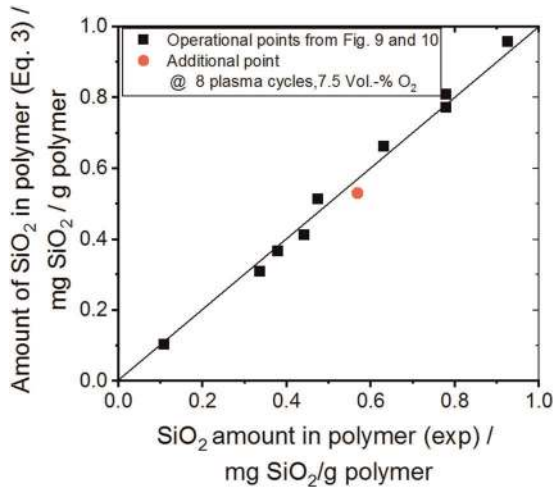
PLASMA PROCESSES AND POLYMERS

FIGURE 11 The amount of nanoparticles deposited determined by experimental values versus that estimated using Equation (3)

mathematical expression to estimate the amount of deposited nanoparticles for any combination of number of plasma cycles and oxygen concentration in the plasma gas using the present setup. The amount of SiO_2 deposited on the surface of the PP particles can be modeled using the following empirical correlation (Equation 2):

$$\left(\text{Amount of } SiO_2 \text{ on polymer}\right) = A \times [\%O_2] \times N$$
$$+ B \times N, \quad (2)$$

where $A = 0.0056 \pm 2.42 \times 10^{-4}$ mg SiO_2/(g polymer·vol.-%O_2), $B = 0.02189 \pm 2.005 \times 10^{-3}$ mg SiO_2/g polymer, N is the number of plasma cycles of 60 s, and $[\%O_2]$ is the oxygen concentration in the plasma gas. Figure 11 shows the calculated amount of SiO_2 deposited on PP using Equation (2) versus the experimentally determined values. The black squares represent the nine points shown

in Figures 9 and 10 used to derive the mathematical equation. An additional point (red circle) was randomly selected to test the accuracy of the model. This point corresponds to a powder coated after eight plasma cycles using 7.5 vol.-%O_2 in the plasma gas.

The results show that the empirical expression predicts the amount of deposited SiO_2 with a reasonable accuracy and can be used to predict the amount of deposited SiO_2 on PP particles of any combination of oxygen concentration and plasma cycles with exception to the case when pure argon is used as a plasma gas. Equation (3) is only valid to predict the amount of silica-like particles deposited on PP particle using the type of materials and the operational conditions described in chapter 2.1. The applicability of this equation to other conditions (e.g., other Si precursor, other polymer particles, different duration of plasma cycles, use of heated bubbler to increase the evaporation of HMDSO, modifications of the reactor) still needs to be analyzed.

3.3 | Influence of the particle coating on the flow properties of PP powders for PBF

A clear correlation between the flow function at different consolidation stresses and the amount of silica nanoparticles determined by ICP-OES can be observed in Figure 12 (left). On the basis of the trend line derived from the different experimental points, the flow function increases with an increasing amount of nanoparticles deposited on the surface until reaching a plateau at about 0.02 wt%. The same trend was observed in all the tested consolidation stresses. As comparison, the flow functions of PP coated with Aerosil® using DPC are also plotted in Figure 12, left (open symbols). These samples were prepared in a way that they replicate the amount of silica nanoparticles and the treatment time of the samples
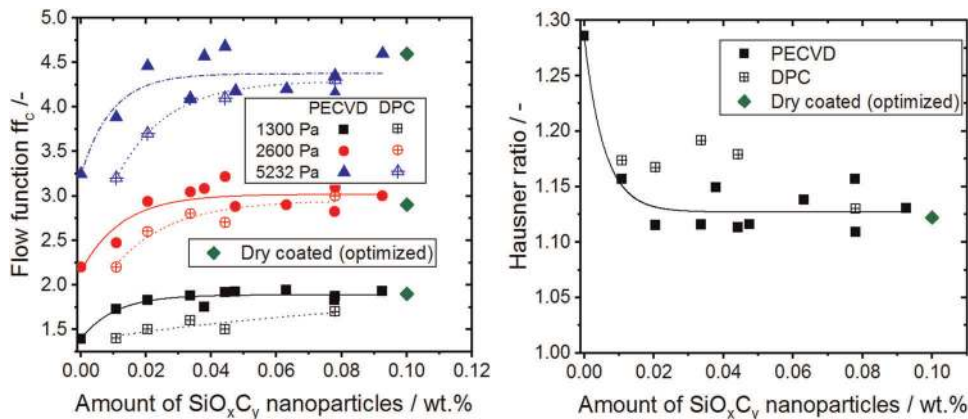

FIGURE 12 Modification of the flow properties of polypropylene powders as a function of the amount of deposited SiO_xC_y particles

produced using a plasma gas concentration of 5 vol.-%O_2 after 2, 4, 6, 8, and 15 min of PECVD treatment. An additional sample produced using 0.1 wt% after 30-min mixing is also analyzed as reference of the flowability, which can be reached by DPC under optimized mixing conditions for the chosen system (same PP powder; 0.1 wt% Aerosil®) using the same tumbling mixer under the same conditions as reported by Blümel.[20] The flow function of the dry coated samples show a similar trend as the PECVD-treated samples: it increases with increasing amount of guest particles at all the three tested consolidations stresses. The flow function (ff_c) of the samples prepared by DPC is lower that the samples prepared by PECVD. The difference between flow functions of the sample prepared by the two methods for similar conditions (treatment time and amount of guest particles) decreases as the amount of guest particles increases. At 0.08 wt% of guest particles (15-min treatment), both methods reached very similar flow functions at the three tested consolidation stresses. The flow function of the sample coated with 0.1 wt% at optimized mixing conditions (green diamonds) is very close the values of the plateaus (at the different consolidation stresses) of the series of samples produced by the plasma treatment. This fact shows that the improvement of the flow behavior of the powder achieved by the presented PECVD process is similar to the one obtained using DPC at optimized conditions.

Analogous to the flow function, the influence of the amount of deposited silica particles on the Hausner ratio of the powders is shown in Figure 12 (right). The Hausner ratio decreases from 1.29 for the raw material to approximately 1.12 at 0.02 wt% when a constant value is reached. The Hausner ratio of the samples treated by DPC with less than 0.045 wt% of Aerosil® oscillates between 1.17 and 1.19, which is connected to the measurement accuracy of the device. For these samples, the Hausner ratio shows a smaller improvement than that achieved by the PECVD process for similar processing time and amount of guest nanoparticles. The sample coated with about 0.08 wt% reached similar results as the sample treated with the presented plasma process for the same process time (5 min). The reference sample coated by DPC at optimized mixing time (30 min) fits well with the values of the Hausner ratio and the trend observed in the samples coated in the fluidized bed.

The better flow behavior and lower Hausner ratio of the samples treated with the PECVD process as compared with the samples treated with DPC with less than 0.78 wt% (<15 min treatment time) of nanoparticles can be explained by the time dependence of the results achieved by DPC. In DPC, a sufficient time of mixing must be provided to deagglomerate the guest nanoparticles added, such that these can be distributed homogenously on the surface of the host particles.[20] The presented plasma process does not show this time dependence, as the nanoparticles are already well dispersed (deagglomerated) on the surface of the host-particles. Thus, for a small amount of guest particles (<0.78 wt%), a more homogenous particle deposition for the same treatment time can be achieved using the PECVD as compared with the DPC. For the deposition of higher amounts of guest particles, which correspond to more than 15-min treatment time, the results obtained by both methods are similar, indicating that the time was sufficient to deagglomerate the nanoparticles of fumed silica in the mixing experiments.

3.4 | Comparison of DPC versus in situ nanoparticle production and particle coating in a fluidized bed

The main difference of the presented process with respect to DPC is the simple time dependence of the coating. As explained by Blümel,[20] the quality of the coating achieved by DPC presents a complex time dependence. At the beginning of the process, the host particles are coated with large sized, inhomogeneously distributed nanoparticle agglomerates. As the mixing time increases, the nanoparticles deagglomerate and redistribute between the different host particles, thus resulting in an increasing number of structures with smaller size and a more homogeneous coating. An optimum is obtained, at which the structures reach a minimum size, whereas the number of structures and the coverage degree reach a maximum. The size, number, and distribution of the nanoparticle agglomerates at the optimum depend strongly on the process parameters such as the type and amount of mixing aids, the mixing device used, the properties of the host and guest particles, and so on.[20,44] A further increase of treatment time from the optimum results in redispersion of the nanoparticle due to the formation of agglomerates of low porosity or mechanofusion of the guest particles on the surface. In the process presented in this investigation, the polymer particles were coated mostly with single nanoparticles and only few sintered aggregates of these single particles rather that with loose agglomerates of nanoparticles. The size of the deposited structures did not change with the time as in DPC. The size distribution of the structures deposited and the degree of coverage achieved are similar to those obtained when using common DPC at the optimal conditions. The number of nanoparticles deposited can be easily controlled by increasing the number of cycles of plasma or by increasing the oxygen concentration in the plasma gas.

The new process combines two individual steps (production of nanoparticles and particle coating) in one process step, which results in a very flexible approach to coat particle with nanoparticles with tailored properties. It allows the in situ production of nanoparticles of different systems (SiO_x, TiO_x, Al_xO_y, Fe_2O_3, carbon) just by changing the type of organic precursor used. This allows to modify the optical, thermal, magnetic, and electric properties of the host material and, in the case of additive manufacturing, the final properties of the produced part. In addition, for a given nanoparticle system, it is possible to tailor the chemical composition, functional groups on the surface, and thus the wetting properties (hydrophilicity/hydrophobicity) of the produced nanoparticles via the composition of the plasma gas. The nanoparticle generation and coating of guest particles in one process step avoid the use of any additional steps for the generation of nanoparticles and the handling of the produced nanoparticles such as transport, packaging, and storage reducing the steps, time, and cost until the final application.

The presented process will require larger times as compared with DPC for the production of core–shell composite particles of polymers coated with large amounts of nanoparticles (>0.1 wt%). However, the efficiency of the process increases when the aim is to coat polymer host particles with small amounts of nanoparticles (<0.1 wt%), for example, to increase the flowability of cohesive powders to be used in PBF, as shown in Section 3.3. In this case, the time necessary to deagglomerate the nanoparticles at the initial step of DPC can be spared, resulting in shorter process times to achieve a homogenous distribution of the particle on the surface of the guest particles.

3.5 | Comparison of in situ nanoparticle production and polymer coating in a fluidized bed versus downstream reactor

Table 5 provides a comparison of the parameter used and the results obtained in this study with those of the studies of Sonnenfeld et al.[23] and Roth et al.[25] where PE-HD powders were treated in a downstream plasma reactor using $Ar/O_2/HMDSO$ mixtures as a plasma gas. This comparison is relevant as PE-HD and PP powders present similar properties (e.g., only carbon and hydrogen in the backbone chain, density, and mean particle size, among others).

For both processes, a considerable increase of the flow function (ff$_c$) with respect to the untreated materials was observed for preconsolidation stresses of approximately 5000 Pa. However, better flowability values were

TABLE 5 Comparison process parameters and flowability results obtained for polyolefins treated in low-pressure downstream reactor

Material	PE-HD	PE-HD	PP
Plasma pressure (bar)	2.00E−03	2.00E−03	1
Plasma powder (W)	100	300	4900
Excitation frequency (MHz)	13.56	13.56	0.021
O_2 concentration (vol.-%)	58	10–40	5–12.5
Flow ratio O_2/HMDSO	10	5–20	0–6.25
Mean host particle size (µm)	55.6	53.8	87.8
Guest particle size (nm)	10–50[26]	10–50[26]	20–350
Flow function ff$_c$ @~5000 Pa	6.5–6.25	5.7–6.25	4.2–4.75
Treatment time (s)	0.1	0.1	60–900
Reference	[23]	[25]	This study

Abbreviations: ff$_c$, flow function; HMDSO, hexamethyldisiloxane; PE-HD, high-density polyethylene.

obtained for the PE-HD powders. The difference in the flowability achieved could be explained by differences in the particle shape, surface roughness at the microscopic and nanoscopic scale (nanoparticles size), surface energy, and coverage degree of the nanoparticles between the treated powders. According to the model of Rumpf,[13] for a given size of host particle, there is an optimum size of guest particles that leads to a minimum of the van der Waals forces. For a host particle with sizes between 50 and 70 µm, this minimum is reached for the nanoparticle with sizes between 10 and 30 nm. In this study, the mean particle size of the silica structures deposited on the surface ranges between 20 and 350 nm, whereas in the the downstream reactor, the size of the deposited agglomerates ranges between 10 and 50 nm.[26] Thus, the size of the nanoaggregates obtained by the downstream plasma reactor is closer to the optimum size interval than the one obtained in the fluidized bed. This could be one of the reasons that explain the better performance. However, it is necessary to investigate more accurately the aforementioned differences between the powders to derive more accurate conclusions.

The process presented in this study using a fluidized bed at atmospheric pressure represents an alternative to coating of micro-sized particles with spacers using the downstream plasma reactor that is operated at low pressures. Both processes have advantages and disadvantages, which have to be weighted to decide which process is more suitable for a given application. The fluidized bed plasma reactor is operated at atmospheric pressure,

simplifying its construction and operation. The operation at atmospheric pressure also avoids the use of more expensive vacuum equipment. The fluidized bed also allows to vary the treatment time of particles easily. In the downer plasma reactors, this is more difficult task, as it will require more passage of the powders through the reactor. However, if the homogeneity of the treatment time is a relevant factor, the downer reactor has a clear advantage, as is characterized by narrow particle residence time distributions and very short process times. Fluidized bed reactors are characterized by excellent mixing, which promotes interparticle interaction between host particle and guest particles, resulting in homogeneous particle coating. The main disadvantage of the fluidized bed plasma reactor is its batch-wise operation as compared with the continuous operation of the downer reactor. The continuous operation of the downstream plasma reactor simplifies the process integration with other steps in the powder production lines. To overcome this disadvantage of the batch-wise operation, the size of the fluidized bed can be easily increased using the well-known scale-up rules[45] and multiple plasma jets could be installed to treat industrially relevant amounts of powder-treated probatch. Thus, both processes are scalable and potentially suitable for use in the industry.

3.6 | Influence of the coating process on the thermal properties of PP powders

To assess the influence of the coating on the crystallization kinetics of the materials, isothermal crystallization measurements at a temperature of 130°C were carried out with
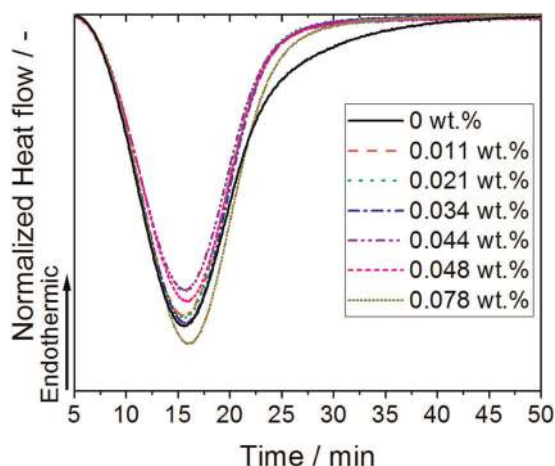

FIGURE 13 Differential scanning calorimetry thermograms of the isothermal measurements, cooling section, of polypropylene powders coated with different amounts of SiO$_x$C$_y$ through plasma-enhanced chemical vapor deposition

the different powders. The results of the isothermal crystallization, as summarized in Figure 13, show no or only minor differences within the samples.

The results of the isothermal crystallization, as shown in Figure 13, show no or only minor differences within the samples. The peak profile of the coated samples is the same or only a few seconds shifted toward larger times than in untreated PP (black curve). This suggests that the low amount of nanoparticles do not act as a nucleating agent during the crystallization of PP. The thermal analysis showed that only negligible effects in the sintering window and crystallization kinetics are observed as consequence of the coating of PP particles with silica nanoparticles for the tested amounts of guest particles. Thus, no difference in the processability of the treated powder in comparison with the raw material is expected.

4 | CONCLUSIONS

Commercial PP powders were coated with silica nanoparticles using a single-step process for the in situ production of nanoparticles using dusty PECVD and mixing in a fluidized bed. The presented process led to the production of nanoparticles of sizes between 10 and 300 nm. The chemical analysis of the nanoparticles revealed that the produced nanoparticles are silica nanoparticles with organic remains (SiO$_x$C$_y$). The organic fraction remaining in the nanoparticles can be reduced by increasing the concentration of oxygen in the plasma gas. Thus, the hydrophobic/hydrophilic properties of the nanoparticles can be easily controlled by the plasma gas composition.

The influences of the oxygen concentration on the plasma gas and the duration of the treatment on the quality of the coating achieved, the amount of nanoparticles deposited on the polymer particles, and the effective conversion were investigated. The results showed that for a given oxygen concentration, the amount of nanoparticles deposited increases linearly with the duration of the treatment (plasma cycles), whereas the effective conversion remains constant. For constant treatment times, the effective conversion, in turn, increases linearly with the oxygen concentration in the plasma gas. Coating of PP powders using pure Argon as plasma gas was not achieved. An empirical model to predict the amount of silica nanoparticles deposited on the PP powders as a function of the treatment time and the oxygen concentration was derived from the linear dependencies found in the analysis.

The effect of the PECVD treatment on the flow properties of the PP powders was investigated. As comparison, a series of samples was prepared by DPC of PP

powders with commercial fumed silica, using the same amount of guest particles and treatment time as in the PECVD-treated samples. All the samples depicted a considerable increase of the flowability of the powders at different consolidation stresses as well as a decrease of the Hausner ratio as compared with the untreated powder. At a low amount of guest particles (<0.078 wt%) and short treatment times (<15 min), the PECVD-treated samples presented better results as compared with the powders treated by DPC. The difference between the flow properties of the powders treated by the two methods decreased with increasing amount of guest particles and treatment time. There was no difference between the flow properties of the powders treated by the PECVD and DPC with 0.078 wt% for 15 min. The PECVD process shows superior results in the terms of flowability in the samples treated with low amounts of silica, which is the normal case of polymer powders used in PBF. Isothermal crystallization measurements showed that the effect of the deposited nanoparticles on the crystallization kinetics of PP is negligible and, thus, no effect on the processability of PP in PBF is expected.

The feasibility study and characterization of the PECVD process were carried out using PP as model material. However, similar results are expected when using other kinds of PBF polymers such as polyamides and polybutylene terephthalate.

ACKNOWLEDGMENTS

CONFLICT OF INTEREST

The authors declare that they have no known competing financial interests or personal relationships that could have appeared to influence the work reported in this paper.

AUTHOR CONTRIBUTIONS

Juan S. Gómez Bonilla: conceptualization, methodology, formal analysis, investigation, writing (original draft), writing (review and editing). **Björn Düsenberg**: formal analysis, writing (original draft). **Franz Lanyi**: formal analysis, writing (original draft). **Patrik Schmuki**: validation, resources. **Dirk W. Schubert**: validation, resources. **Jochen Schmidt**: conceptualization, methodology, formal analysis, writing (original draft), writing (review and editing), project administration. **Wolfgang Peukert**: methodology, validation, resources, formal analysis. **Andreas Bück**: conceptualization, methodology, validation, resources, writing (original draft), writing (review and editing), project administration.

DATA AVAILABILITY STATEMENT

The data that support the findings of this study are available from the corresponding author upon reasonable request.

ORCID

Juan S. Gómez Bonilla https://orcid.org/0000-0002-9670-9289
Patrik Schmuki https://orcid.org/0000-0002-9208-5771
Jochen Schmidt https://orcid.org/0000-0002-9056-2749
Wolfgang Peukert https://orcid.org/0000-0002-2847-107X
Andreas Bück http://orcid.org/0000-0002-7803-1486

REFERENCES

[1] a) I. Gibson, D. Rosen, B. Stucker, *3D Printing, Rapid Prototyping and Direct Digital Manufacturing*, 2nd ed., Springer, New York, Heidelberg, Dodrecht, London **2015**; b) T. T. Wohlers, T. Caffrey, R. I. Campbell, *3D Printing and Additive Manufacturing State of the Industry: Annual Worldwide Progress Report*, Wohlers Associates, Fort Collins, CO **2016**.

[2] a) M. Schmid, *Technology, Processes, and Materials*, 1st ed., Hanser Publishers, Munich, Germany **2018**; b) S. C. Ligon, R. Liska, J. Stampfl, M. Gurr, R. Mülhaupt, *Chem. Rev.* **2017**, *117*, 10212.

[3] A. M. Stoklosa, R. A. Lipasek, L. S. Taylor, L. J. Mauer, *Food Res. Int.* **2012**, *49*, 783.

[4] J. K. Prescott, R. A. R. Barnum, *Pharm. Technol.* **2000**, *24*, 60.

[5] a) G. Xu, P. Lu, M. Li, C. Liang, P. Xu, D. Liu, X. Chen, *Exp. Therm. Fluid Sci.* **2018**, *92*, 390; b) M. Götzinger, W. Peukert, *Powder Technol.* **2003**, *130*, 102; c) D. Schiochet Nasato, T. Pöschel, *Addit. Manuf.* **2020**, *36*, 101421.

[6] Q. Li, V. Rudolph, B. Weigl, A. Earl, *Int. J. Pharm.* **2004**, *280*, 77.

[7] a) N. Mys, R. van de Sande, A. Verberckmoes, L. Cardon, *Polymers* **2016**, *8*, 150; b) N. Mys, A. Verberckmoes, L. Cardon, *Polymers* **2016**, *8*, 383.

[8] J. S. Gomez Bonilla, M. A. Dechet, J. Schmidt, W. Peukert, A. Bück, *Rapid Prototyping J.* **2020**, *26*, 1637.

[9] J. Schmidt, M. Sachs, S. Fanselow, M. Zhao, S. Romeis, D. Drummer, K.-E. Wirth, W. Peukert, *Chem. Eng. Sci.* **2016**, *156*, 1.

[10] a) I. Zimmermann, M. Eber, K. Meyer, *Z. Phys. Chem.* **2004**, *218*, 51; b) T. Kojima, J. A. Elliott, *Chem. Eng. Sci.* **2013**, *101*, 315.

[11] C. Blümel, M. Sachs, T. Laumer, B. Winzer, J. Schmidt, M. Schmidt, W. Peukert, K.-E. Wirth, *Rapid Prototyping J.* **2015**, *21*, 697.

[12] M. M. Lexow, D. Drummer, *J. Powder Technol.* **2016**, *2016*, 4101089.

[13] H. Rumpf, *Chemie Ing. Tech.* **1974**, *46*, 1.

[14] A. Spillmann, A. Sonnenfeld, P. R. von Rohr, *Plasma Processes Polym.* **2008**, *5*, 753.

[15] M. A. Dechet, A. Demina, L. Römling, J. S. Gómez Bonilla, F. J. Lanyi, D. W. Schubert, A. Bück, W. Peukert, J. Schmidt, *Addit. Manuf.* **2020**, *32*, 100966.

[16] X. L. Jiang, S. J. Luo, K. Sun, X. D. Chen, *eXPRESS Polym. Lett.* **2007**, *1*, 245.

[17] R. G. Kleijnen, M. Schmid, K. Wegener, *AIP Conf. Proc.* **2016**, *1779*, 100004.

[18] E. D. Bain, E. J. Garboczi, J. E. Seppala, T. C. Parker, K. B. Migler, *Integr. Mater. Manuf. Innov.* **2019**, *8*, 335.

[19] R. Pfeffer, R. N. Dave, D. Wei, M. Ramlakhan, *Powder Technol.* **2001**, *117*, 40.

[20] C. Blümel, Charakterisierung der Trockenen Beschichtung zur Herstellung von maßgeschneiderten Kompositpartikeln. Zugl.: Erlangen-Nürnberg, Univ., Diss., 2015, 1. Aufl. ed., Verl. Dr. Hut, München, 2015.

[21] a) D. Zhang, B. Gökce, S. Barcikowski, *Chem. Rev.* **2017**, *117*, 3990; b) T. Sugimoto, X. Zhou, A. Muramatsu, *J. Colloid Interface Sci.* **2003**, *259*, 53; c) S. Barcikowski, A. Menéndez-Manjón, B. Chichkov, M. Brikas, G. Račiukaitis, *Appl. Phys. Lett.* **2007**, *91*, 83113; d) F. Kruis, H. Fissan, A. Peled, *J. Aerosol Sci.* **1998**, *29*, 511.

[22] A. Sonnenfeld, C. Roth, Z. Dimitrova, A. Spillmann, P. R. von Rohr, *Plasma Processes Polym.* **2009**, *6*, S860.

[23] A. Sonnenfeld, A. Spillmann, C. Arpagaus, P. Rudolf von Rohr, *Plasma Processes Polym.* **2009**, *6*, 170.

[24] A. Spillmann, A. Sonnenfeld, P. R. von Rohr, *Plasma Processes Polym.* **2007**, *4*, S16.

[25] C. Roth, A. Sonnefeld, P. R. von Rohr, in Proceedings of the 19th International Symposium on Plasma Chemistry (ISPC 19), **2009**.

[26] C. Roth, *PhD Thesis*, ETH Zurich **2012**.

[27] C. Arpagaus, G. Oberbossel, P. R. von Rohr, *Plasma Processes Polym.* **2018**, *15*, 1800133.

[28] M. Sachs, J. Schmidt, W. Peukert, K.-E. Wirth, *Powder Technol.* **2018**, *325*, 490.

[29] J. S. Gómez Bonilla, T. Szymczak, X. Zhou, S. Schrüfer, M. A. Dechet, P. Schmuki, D. W. Schubert, J. Schmidt, W. Peukert, A. Bück, *Addit. Manuf.* **2020**, *34*, 101373.

[30] J. S. Gómez Bonilla, H. Trzenschiok, F. Lanyi, D. W. Schubert, A. Bück, J. Schmidt, W. Peukert, in Proceedings of the 30th Annual International Solid Freeform Fabrication Symposium, **2019**.

[31] J. Schmidt, E. J. Parteli, N. Uhlmann, N. Wörlein, K.-E. Wirth, T. Pöschel, W. Peukert, *Adv. Powder Technol.* **2020**, *31*, 2293.

[32] R. Wallimann, C. Roth, P. R. von Rohr, *Plasma Processes Polym.* **2018**, *15*, 1700202.

[33] C. Roth, G. Oberbossel, E. Buitrago, R. Heuberger, P. R. von Rohr, *Plasma Processes Polym.* **2012**, *9*, 119.

[34] A. Bouchoule (Ed.) *Dusty plasmas. Physics, chemistry, and technological impacts in plasma processing*, Wiley, Chichester, **1999**.

[35] J. Schäfer, R. Foest, A. Quade, A. Ohl, K.-D. Weltmann, *J. Phys. D: Appl. Phys.* **2008**, *41*, 194010.

[36] P. G. Pai, S. S. Chao, Y. Takagi, G. Lucovsky, *J. Vac. Sci. Technol., A* **1986**, *4*, 689.

[37] S. M. Han, E. S. Aydil, *J. Vac. Sci. Technol., A* **1996**, *14*, 2062.

[38] A. Grill, D. A. Neumayer, *J. Appl. Phys.* **2003**, *94*, 6697.

[39] M. Jaritz, C. Hopmann, H. Behm, D. Kirchheim, S. Wilski, D. Grochla, L. Banko, A. Ludwig, M. Böke, J. Winter, H. Bahre, R. Dahlmann, *J. Phys. D: Appl. Phys.* **2017**, *50*, 445301.

[40] J. Schäfer, R. Foest, A. Quade, A. Ohl, K.-D. Weltmann, *Plasma Processes Polym.* **2009**, *6*, S519.

[41] P. Raynaud, B. Despax, Y. Segui, H. Caquineau, *Plasma Processes Polym.* **2005**, *2*, 45.

[42] C. T. Rueden, J. Schindelin, M. C. Hiner, B. E. DeZonia, A. E. Walter, E. T. Arena, K. W. Eliceiri, *BMC Bioinf.* **2017**, *18*, 529.

[43] C. Anh Ho, M. Sommerfeld, *Chem. Eng. Sci.* **2002**, *57*, 3073.

[44] J. Yang, A. Sliva, A. Banerjee, R. N. Dave, R. Pfeffer, *Powder Technol.* **2005**, *158*, 21.

[45] a) M. Rüdisüli, T. J. Schildhauer, S. M. Biollaz, J. R. van Ommen, *Powder Technol.* **2012**, *217*, 21; b) T. M. Knowlton, S. Karri, A. Issangya, *Powder Technol.* **2005**, *150*, 72.